ChemComm

COMMUNICATION

View Article Online
View Journal | View Issue

Cite this: *Chem. Commun.*, 2025, **61**, 7281

Received 25th February 2025,
Accepted 3rd April 2025

DOI: 10.1039/d5cc00380f

rsc.li/chemcomm

Structural isomers of imine-linked covalent organic cages with divergent photocatalytic properties†

Jiajia Li,‡[ab] Yanping Yang,‡[ab] Shan Shiang Hii,[a] Xinyuan Zhu [a] and Youfu Wang *[a]

The impact of linkage orientation as structural isomers on the properties of covalent organic cages (COCs) has been investigated. Isomeric imine-linked COCs, featuring triphenylamine as the donor and anthracene as the acceptor, TNCA and TCNA, were synthesized and exhibited significant differences in their optoelectronic properties, which in turn affect their photocatalytic performance.

As emerging giant molecules, covalent organic cages (COCs) with precise, discrete, and steric nanostructures are typically constructed from organic building blocks through reversible covalent bonds to improve the yields of multi-site reactions.[1] Thanks to the principles of reticular chemistry, COCs can be designed and synthesized in a predictable manner.[2,3] Over the past decades, various novel COCs with unique building blocks and linkages have been developed to endow the designable structures and controllable properties for diverse applications.[4,5] However, the significant structural variation in the linkages, particularly their orientation, has not been thoroughly explored in the context of COCs. This issue has been noticed in covalent organic frameworks (COFs) connecting through similar reticular chemistry with COCs and several studies have been conducted to prove the critical impact of the linkage orientation on the overall properties, especially for the optoelectronic properties.[6–9] However, the ubiquitous 2D stacking or 3D interpenetration and inevitable defects may obscure the structure–property relationship in COFs.[10] Therefore, studying the structural isomerism of COCs can reveal this structure–property relationship more profoundly to direct the structural design and property regulation of COCs (Table S1, ESI†).

To verify the impact of linkage orientation in COCs on their properties, the well-studied imine linkage is selected because it is easy to synthesize and possess good chemical stability.[11] Structural isomerism in linkages is particularly significant for donor–acceptor (D–A) type COCs, which are extensively studied for optoelectronic and photocatalytic applications, where the interaction between donor and acceptor moieties is crucial to their properties and performance.[12]

Due to its exceptionally high hole mobility, triphenylamine has emerged as a prominent electron-donating group.[13] Additionally, the rigid anthracene module, with its abundant photo-responsive properties, adds significant interest.[14] We synthesized isomeric imine-linked COCs with triphenylamine (T) as the donor and anthracene (A) as the acceptor, namely TNCA and TCNA, to examine and compare their structural, optoelectronic, and photocatalytic properties. Single crystal structures, molecular orbital calculations, and optical and electrochemical analyses reveal that TNCA demonstrates superior light absorption, a lower bandgap, enhanced charge separation efficiency, and improved photocatalytic dye degradation performance. This study underscores that structural isomerism in COCs, even with minor structural changes, is a prevalent factor and should be carefully considered in the design and optimization of COCs for specific applications (Scheme 1).

Triphenylamine and 1,8-disubstituted anthracene were utilized to synthesize triangular prism-shaped COC isomers, TNCA and TCNA, through Schiff base reactions, achieving moderate yields of 74% and 45%, respectively. Structural confirmation of COC isomers and intermediates was performed using nuclear magnetic resonance (NMR) spectra, Fourier transform infrared (FT-IR) spectra, and high-resolution mass spectra (HRMS) (Fig. S1–S13, ESI†). The ^{1}H NMR spectra show a single set of resonances for TNCA and TCNA, indicating highly symmetric structures. Specifically, the –HC═N– (Hc) signals appear at 9.42 ppm for TNCA and 8.65 ppm for TCNA, confirming the expected formation of these isomers. The solid-state ^{13}C CP/MAS NMR analyses show that the imine carbon signals of TNCA and TCNA exhibit minor chemical

[a] *School of Chemistry and Chemical Engineering, Shanghai Jiao Tong University, Shanghai 200240, China. E-mail: wyfown@sjtu.edu.cn*
[b] *School of Materials Science and Engineering, Shanghai University of Engineering Science, Shanghai 201620, China*

† Electronic supplementary information (ESI) available. CCDC 2375696 and 2375697. For ESI and crystallographic data in CIF or other electronic format see DOI: https://doi.org/10.1039/d5cc00380f

‡ These authors have contributed equally.

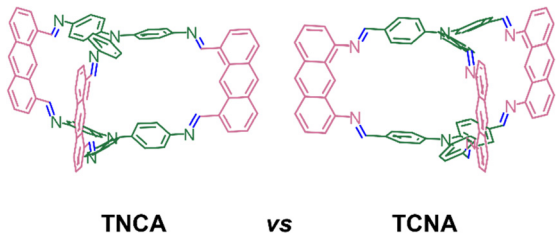

Scheme 1 Structures of D–A COC isomers with reversed orientation of imine linkage.

shifts at 161 and 159 ppm, respectively. Furthermore, the carbon nuclei adjacent to the imine nitrogen atoms resonate at 148 ppm (TNCA) and 151 ppm (TCNA), providing additional evidence for the unique electronic environment of the imine bonds within COC isomers (Fig. 1a and Fig. S9, S11, S13, ESI†). HRMS data supports the [2+3] cage structure with molecular weights m/z = 1175.4592 for TNCA and m/z = 1175.4822 for TCNA, consistent with the simulated mass (m/z = 1175.4544) for molecular formula of $C_{84}H_{54}N_8$ (Fig. S10 and 12, ESI†). FT-IR spectra reveal distinct –C═N– stretching signals at 1626 and 1608 cm^{-1} for TNCA, and 1628 and 1593 cm^{-1} for TCNA, reflecting the different chemical environments of the imine linkages (Fig. 1b and Fig. S14, ESI†).[15] UV-Vis and photoluminescence spectra show TNCA absorbing at 453 nm (32 nm red shift compared to TCNA) and emitting at 467 nm (8 nm blue shift compared to TCNA). The narrow emission spectra and small Stokes shift (13 nm for TNCA and 54 nm for TCNA) suggest limited structural relaxation, dominant role of anthracene arms in electronic transitions, and orientation-dependent absorption and luminescence behavior.[16] The transient fluorescence lifetime results showed that the average fluorescence lifetime of TNCA is 1.12 ns, significantly shorter than that of TCNA (2.47 ns). This indicated that, under light excitation, TNCA efficiently generates photogenerated charge carriers, allowing their rapid migration to the reaction sites and converting light energy into chemical energy to enhance the photocatalytic reaction.[17] The differences in color (brown-red for TNCA, orange for TCNA), absorption, and emission behaviors indicate that the –C═N– linkage orientation affects electronic characteristics (Fig. S15–S18, ESI†).

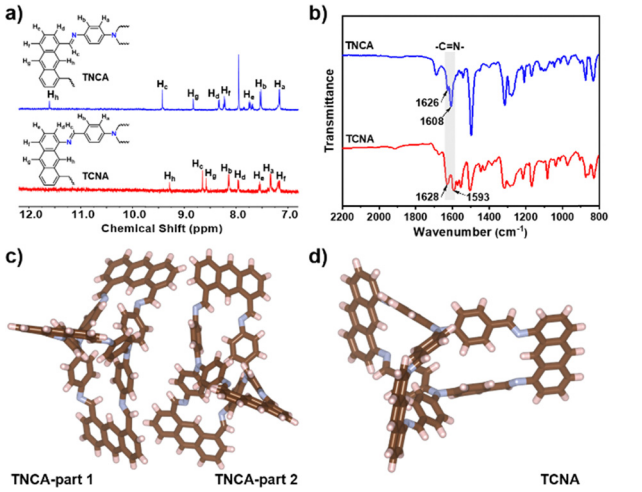

Fig. 1 Structural characterization of COC isomers. (a) ^{1}H NMR spectra of TNCA and TCNA in DMSO-d_6. (b) FT-IR spectra of TNCA and TCNA. (c) and (d) Crystal structures of TNCA and TCNA.

Through the slow solvent diffusion method, needle-shaped crystals of the COC isomers were obtained (Fig. S19, ESI†). Analysis of the single crystal structures reveals that the TNCA crystal belongs to the monoclinic system with a $P2_1/n$ space group and a unit cell volume of 8284.2(3) Å^3. In contrast, the TCNA crystal belongs to the triclinic system, with a $P\bar{1}$ space group and a unit cell volume of 9619.9(6) Å^3. Notably, the anthracene groups in the TNCA crystals exhibited a degree of freedom, leading to two distinct configurations. The solution mask routine in Olex2 was employed to address the severely disordered regions. The anthracene unit was disordered over two sites, each with an occupancy of 0.5. Specifically, in the TNCA-part 1 structure, four C═N linkages connecting two anthracene arms were oriented inward toward the COC cavity. However, the two C═N linkages connecting the third anthracene arm were oriented in other ways: one pointed inward and the other outward. Conversely, in the TNCA-part 2 structure, only two C═N linkages from one anthracene arm pointed inward toward the COC cavity, while the remaining two pairs of C═N linkages, connecting the other two anthracene arms, were arranged with one pointing inward and one pointing outward. In the TCNA crystal structure, all six C═N linkages were directed inward toward the COC cavity. In all cases, the needle-shaped crystals have been confirmed to be triangular prismatic [2+3] cages with large cavities (Fig. 1c, d and Fig. S20, Table S2, ESI†).

We also investigated the UV-Vis diffuse reflectance spectra (DRS) of COC isomers in the solid state under both dark and light irradiation conditions. TNCA and TCNA both exhibit broad light absorption, with onset edges at 1500 nm and 870 nm, respectively (Fig. S21, ESI†). The optical energy band gaps (E_g), calculated from Tauc plots,[18] reveals that TNCA had a narrower gap (2.04 eV) compared to TCNA (2.10 eV) under dark (Fig. 2a). Upon light irradiation (Xe lamp with 420 nm cutoff filter, 300 W), the absorption intensity of the COC powders increases notably. With broader absorption range and higher absorption intensity, TNCA demonstrates superior light utilization efficiency, evidenced by its reduced optical band gap and extraordinarily minimal Stokes shift.

To evaluate the electrochemical performance and redox capabilities of the COC isomers, we conducted a series of measurements including cyclic voltammetry (CV), electrochemical impedance spectroscopy (EIS) Nyquist plots, and Mott–Schottky (M–S) analysis. The CV curves reveal that the onset oxidation potentials for TNCA and TCNA are 0.36 V and 1.14 V, respectively. The initial reduction potentials are −0.78 V for TNCA and −0.81 V for TCNA (Fig. S22, ESI†). These results indicate that TNCA undergoes redox reactions more readily and exhibits higher electrochemical activity compared to TCNA.[16] EIS Nyquist plots further demonstrate that TNCA has lower electrochemical impedance and smaller charge transfer

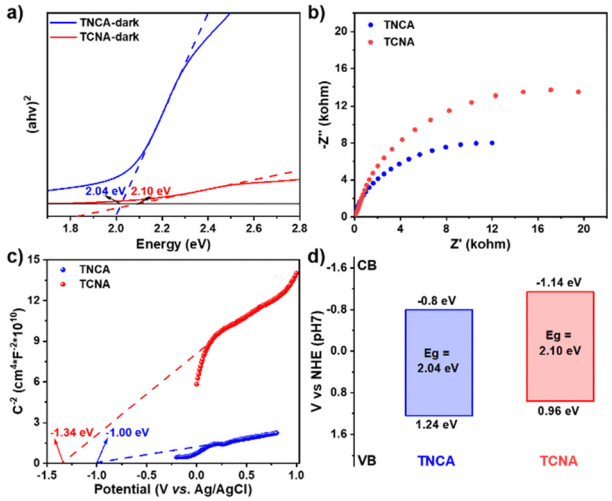

Fig. 2 Optoelectrical properties of COC isomers. (a) Tauc plots. (b) EIS Nyquist plots. (c) M–S plots. (d) Band structures.

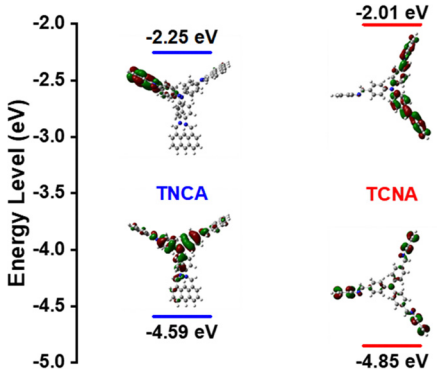

Fig. 3 Energy diagrams and visual representations of the frontier molecular orbitals of TNCA and TCNA.

resistance, suggesting superior charge transport properties (Fig. 2b). To further explore the band structures of the COC isomers, we performed M–S analysis to determine the conduction band (E_{CB}) and valence band (E_{VB}) values, complementing the E_g values obtained from Tauc plots. The M–S plots for TNCA and TCNA exhibit a positive slope (Fig. 2c and Fig. S23, ESI†), indicative of typical n-type semiconductor behavior.[19] This aligns with the expectation that the triphenylamine unit within the conjugated skeleton facilitates electron transport. The flat band potential of an n-type semiconductor is closer to the conduction band position.[20] Accordingly, the E_{CB} values are estimated to be −0.8 V for TNCA and −1.14 V for TCNA. The E_{VB} values are calculated as 1.24 V for TNCA and 0.96 V for TCNA (*vs.* NHE, pH 7) using the equation $E_{CB} = E_{VB} - E_g$ (Fig. 2d).[9] Overall, these findings demonstrate that TNCA exhibits superior optical and electrochemical performance compared to TCNA, with greater efficiency in charge separation and transfer. The results further illustrate how the optoelectronic properties of COCs can be finely tuned by changing the C=N linkage orientation.

For TNCA and TCNA, frontier orbital energy levels are computed to gain deeper insights. Time-dependent density functional theory (TD-DFT) with the B3LYP/6-31G(d,p) basis set is employed for geometrical optimizations and determining molecular orbital energy levels.[7] The estimated highest occupied molecular orbitals (HOMO) for TNCA and TCNA are −4.59 eV and −4.85 eV, respectively, while the lowest unoccupied molecular orbitals (LUMO) are −2.25 eV and −2.01 eV. TNCA exhibits stronger redox capabilities and then is more easily excited compared to TCNA, consistent with the CV curves. The simulated HOMO–LUMO gap values of 2.34 eV for TNCA and 2.84 eV for TCNA align well with the trend observed in the experimental bandgap (E_g) values calculated from the Tauc plot (TNCA: 2.04 eV, TCNA: 2.10 eV). This suggests that TNCA is more efficient in generating electrons and facilitates electron–hole pair separation under photoexcitation, benefiting from its superior light absorption capability. In TNCA, the HOMO is delocalized over the triphenylamine caps and adjacent C=N linkages, while in TCNA, the HOMO is localized on the anthracene arms. Although the LUMO in both isomers is mainly located on the anthracene arms and adjacent C=N linkages, it is concentrated on one anthracene arm in TNCA and spread across two arms in TCNA (Fig. 3 and Fig. S24, ESI†). This indicates the crucial influence of the C=N linkage orientation on the energy levels, redox properties, and electronic density distribution of the final COCs with similar skeletons.

To verify the hypothesis regarding the different photocatalytic properties of these COC isomers, we further measured the photocurrent (*i*–*T*) and electron paramagnetic resonance (EPR) spectra to evaluate their photo-responsibility. Notably, a significant EPR signal at *g*-factor = 2.000 in the dark is observed, indicating that both TNCA and TCNA possess intrinsic electron–hole pair signals.[21] This suggests that COC isomers have a certain capacity for electron–hole separation. The EPR signal of TNCA is slightly stronger than that of TCNA, and under identical light irradiation conditions, the EPR signals of both COC isomers are enhanced, consistent with the enhanced absorption in DRS (Fig. 4a). The *i*–*T* plots confirm that the COC isomers are n-type semiconductors with electrons as the majority of the photo-generated carriers, as evidenced by their positive transient photocurrents.[9] The dark current densities are 4.48 μA cm^{-2} for TNCA and 3.06 μA cm^{-2} for TCNA, demonstrating their potential for electron transport. The maximum photocurrent densities are 6.29 μA cm^{-2} for TNCA and 3.67 μA cm^{-2} for TCNA, aligning with the trends observed in EIS plots and the photo-responsive EPR results (Fig. 4b). These findings suggest that the COC isomers may possess photocatalytic properties, with TNCA showing superior light absorption capability and higher charge separation efficiency, supporting its potential for subsequent dye photodegradation applications.

Finally, we assessed the capability of the COC isomers for photocatalytic degradation of organic dyes. Two representative dyes, methylene blue trihydrate (MBT) and rhodamine B (RhB), are chosen due to their minimal optical absorption overlap with the COC isomers. Without a photocatalyst, the degradation rate of MBT after 20 minutes of irradiation is only about

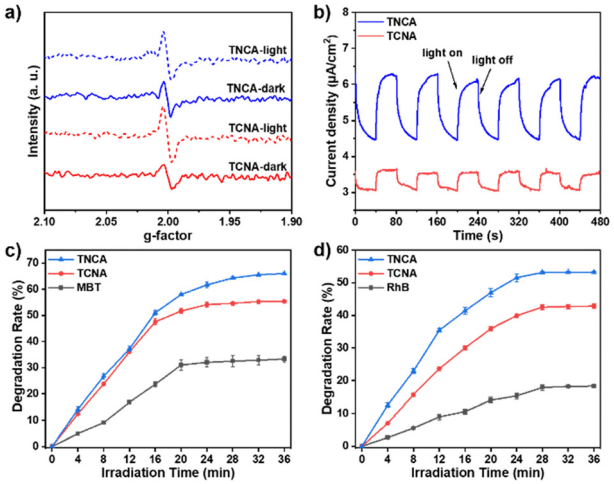

Fig. 4 The dye photodegradation performance of COC isomers as photocatalyst. (a) The EPR spectra of COC isomers under dark and light irradiation conditions. (b) *i*–*T* plots of COC isomers. (c) and (d) Degradation of MBT and RhB under light irradiation with and without COC isomers as photocatalyst.

33%. However, this rate significantly increases in the presence of COC isomers: TNCA achieves a maximum degradation of 66% and TCNA 55%. A similar trend is observed for RhB, with degradation rates rising from 18% without COC to 53% with TNCA and 43% with TCNA (Fig. 4c, d and Fig. S25, ESI†). Moreover, the COC isomers maintain outstanding reusability for the photodegradation. The FT-IR spectra of COC isomers after photocatalysis revealed no observable new peaks or bond cleavage, indicating the COC isomers were structurally stable after photocatalysis (Fig. S26 and S27, ESI†). The COC isomer also exhibit excellent thermal stability and photochemical stability. From thermogravimetric analysis (TGA) plots, TNCA begins to show significant weight loss around 480 °C, while TCNA at 430 °C (Fig. S28, ESI†). Specially, COC solutions in dichloromethane demonstrated remarkable photostability, showing negligible variation of absorption plots during prolonged 120 min irradiation (Fig. S29, ESI†). Additionally, EPR tests confirm the formation of superoxide anions ($O_2^{\bullet-}$) and hydroxyl radicals ($^{\bullet}OH$) through scavenging by 5-dimethyl-1-pyrroline *N*-oxide (DMPO) under visible light irradiation, indicating that COC isomers can generate reactive oxygen species (ROS) to enhance the photocatalytic activity (Fig. S30, ESI†). A brief mechanistic pathway for dye photodegradation is proposed. Upon light exposure, the intrinsic electron–hole pair can directly degrade dyes. Electron transit from the valence to conduction band, subsequently reacting with oxygen to generate $O_2^{\bullet-}$. Simultaneously, the photogenerated holes oxidize trace amounts of water present to produce $^{\bullet}OH$. These ROS synergistically enhance the degradation efficiency of dyes (Fig. S31, ESI†). Specifically, with optimal orientation of imine linkage, TNCA's lower bandgap, high electron–hole transport efficiency, and reduced electron–hole recombination, contributed to its superior photocatalytic performance.

In summary, we suggest that the orientation of chemical linkages in COCs should be given as much attention as the backbone functionalities when designing these materials. Using the imine linkage, the most commonly studied in COC chemistry, we investigated its isomerism effect in donor–acceptor COCs. We synthesized two COC isomers, TNCA and TCNA, with identical skeletons but opposite orientations of the imine linkage. Both experimental results and DFT simulations highlight the significant impact of imine linkage orientation on the optoelectronic properties and photocatalytic dye degradation performance of the COC isomers. This study demonstrates that atomic-level structural adjustments, particularly bond orientation and isomerism, critically govern the band structure and photocatalytic activity of COCs, enabling tailored designs for pollutant-specific degradation (*e.g.*, antibiotics, heavy metals). The established "bond orientation-band structure–activity" model not only deciphers COC structure–property relationships but also offers a transferable strategy to optimize diverse linkages in COC-based materials.

This work was supported by the Class III Peak Discipline of Shanghai-Materials Science and Engineering (High Energy Beam Intelligent Processing and Green Manufacturing).

Data availability

The data supporting this article have been included as part of the ESI.†

Conflicts of interest

There are no conflicts to declare.

Notes and references

1 X. Yang, Z. Ullah and J. F. Stoddart, *et al.*, *Chem. Rev.*, 2023, **123**, 4602–4634.
2 O. M. Yaghi, *ACS Cent. Sci.*, 2019, **5**, 1295–1300.
3 J. Li, S. S. Hii and X. Zhu, *et al.*, *Chin. Chem. Lett.*, 2025, **36**, 111151.
4 J. Li, Y. Yang and J. Yang, *et al.*, *Coord. Chem. Rev.*, 2025, **523**, 216260.
5 D. Cui, F. Bai and L. Zhang, *et al.*, *Angew. Chem., Int. Ed.*, 2024, **63**, e202319815.
6 J. Yang, S. Ghosh and J. Roeser, *et al.*, *Nat. Commun.*, 2022, **13**, 6317.
7 X. Ren, M. Wen and X. Hou, *et al.*, *Chem. Commun.*, 2024, **60**, 4423–4426.
8 H. He, *J. Mater. Chem. A*, 2024, **12**, 227–232.
9 W. Dong, Z. Qin and K. Wang, *et al.*, *Angew. Chem., Int. Ed.*, 2023, **62**, e202216073.
10 S. Daliran, M. Blanco and A. Dhakshinamoorthy, *et al.*, *Adv. Funct. Mater.*, 2024, **34**, 2312912.
11 J. Kou, Q. Wu and D. Cui, *et al.*, *Angew. Chem., Int. Ed.*, 2023, **62**, e202312733.
12 L. Chen, C. Li and Z.-F. Liu, *et al.*, *Chem. Commun.*, 2024, **60**, 1758–1761.
13 D. Wang, L. Zhang and Y. Zhao, *J. Org. Chem.*, 2022, **87**, 2767–2772.
14 G.-H. Ning, P. Cui and I. V. Sazanovich, *et al.*, *Chem*, 2021, **7**, 3157–3170.
15 M. Wilms, D. Tibben and I. Lyskov, *et al.*, *J. Phys. Chem. C*, 2024, **128**, 15041–15047.
16 S. Ghosh, Y. Tsutsui and K. Suzuki, *et al.*, *Mol. Syst. Des. Eng.*, 2019, **4**, 325–331.
17 Y. Yang, H. Niu and L. Xu, *et al.*, *Appl. Catal., B*, 2020, **265**, 118799.
18 J.-R. Wang, K. Song and T.-X. Luan, *et al.*, *Nat. Commun.*, 2024, **15**, 1267.
19 S.-M. Yi, C.-R. Zhang and X. Liu, *et al.*, *Chem. Eng. J.*, 2023, **475**, 146264.
20 Y. Li, L. Yang and H. He, *et al.*, *Nat. Commun.*, 2022, **13**, 1355.
21 J. Yang, A. Acharjya and M. Ye, *et al.*, *Angew. Chem., Int. Ed.*, 2021, **60**, 19797–19803.

